

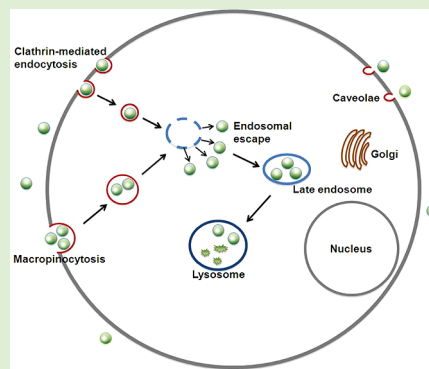
Endocytic Uptake and Intracellular Trafficking of Bis-MPA-Based Hyperbranched Copolymer Micelles in Breast Cancer Cells

Xianghui Zeng, Yuning Zhang, and Andreas M. Nyström*

Swedish Medical Nanoscience Center, Department of Neuroscience, Karolinska Institutet, Retzius väg 8, SE-171 77, Stockholm, Sweden

S Supporting Information

ABSTRACT: Dendrimers and their less well-defined cousins, hyperbranched polymers, are widely investigated as scaffold materials in tissue engineering, as drug delivery agents, and in diagnostic imaging applications. Despite the large interest of using these unique materials as polymer-based nanoparticles in biomedical applications, a clear understanding of the cellular uptake and transport of these polyester-based nanoparticles is still lacking. The objective of this study is to evaluate the cellular uptake profiles and intracellular trafficking of polymer micelles built from the hyperbranched polyester Boltorn, fitted with poly(ethylene glycol) and fluorescent groups in MDA-MB468 breast cancer cells. Results show that the uptake of these nanoparticles correlated positively to both time and concentration, and that the uptake of the nanoparticles was energy dependent. These polyesterbased nanoparticles appear to translocate across cells via clathrin- and macropinocytosis-mediated endocytosis. Observations of the intracellular trafficking of the nanoparticles indicate that particles could be released from early endosomes after being internalized, and the particles exhibit perinuclear localization. The uptake behavior of the nanoparticles was further evaluated in a range of cell lines. These results allow the generation of the knowledge base required to design polyester-based nanocarriers that can be used efficiently and specifically for drug delivery applications and imaging applications.



INTRODUCTION

Polymer materials have emerged as one of the most versatile construction materials for nanoscale systems in biomedical applications.^{1–3} Dendrimers and hyperbranched polymers represent a unique architectural class of polymers used in nanomedical applications, and possess a highly branched structure, a multitude of available surface groups, as well as improved solubility as compared to their linear analogues.⁴ Several engineered dendrimers are now being developed as candidates for therapeutic and diagnostic applications in medicine.^{5–7} Boltorn is a hyperbranched aliphatic polyester based on the poly-2,2-bis(methylol) propionic acid (bis-MPA) monomer unit. Boltorn is a viable model system resembling dendrimers in drug delivery applications, as these aliphatic hyperbranched polymers retain many of the unique properties of the polyester dendrimer structure, including its nontoxic properties, but without the complex multistep synthesis process. The group of Fréchet et al. have spent considerable efforts to develop bis-MPA-based dendrimers for nanomedical applications, including dendrimers for targeted positron emission tomography (PET) imaging, as well as very efficient drug delivery carriers of doxorubicin (DOX) *in vivo*.^{8,9} Recent elegant studies by Gong et al. have used Boltorn hyperbranched carriers in cancer therapy and showed promising results in drug encapsulation and controlled release behavior.^{10–15} It has been confirmed recently that bis-MPA-based dendrimers are degradable, biocompatible, and do not display cytotoxicity or

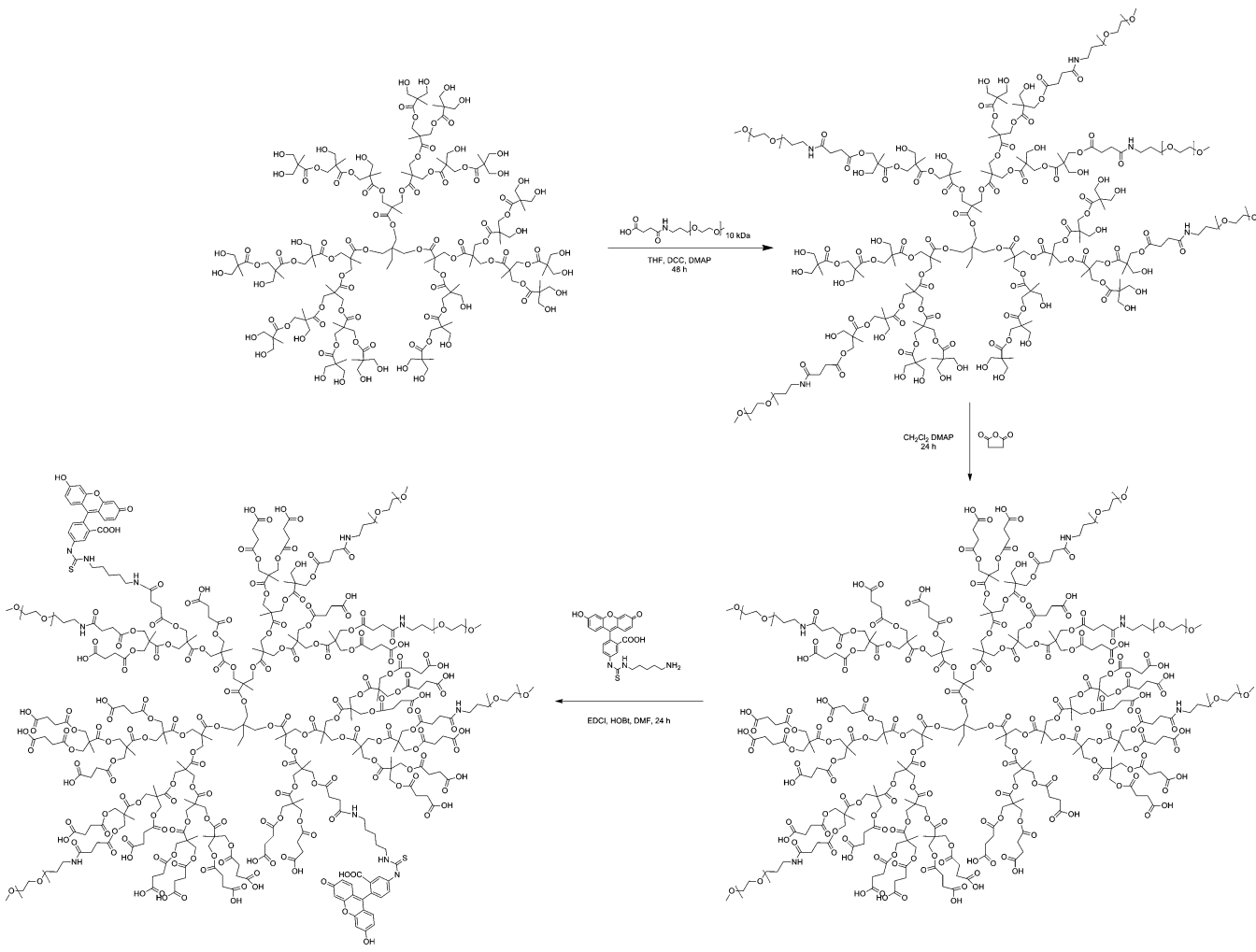
immunogenicity to human cancer cell lines and primary cells.^{11,16}

We are interested in developing a simple process that enables the formation of polymer nanoparticles from a two-component Boltorn–poly(ethylene glycol) (PEG) copolymer system in order to rapidly be able to test the formulation of both clinically used chemotherapeutics and novel drug candidates in volumes relevant for preclinical development. Our copolymer system avoids the multistep synthesis process used for dendrimers, and the hyperbranched polymer nanoparticles are formulated via self-assembly.¹⁷ Our laboratory recently reported on the drug release profiles of polymer micelles based on copolymers of Boltorn and PEG (Boltorn-H30-*co*-(PEG_{10k})₅ with variable sizes of the Boltorn core (H30 and H40) and the PEG chains (PEG5k and PEG10k). The Boltorn-H30-*co*-(PEG_{10k})₅ containing physically entrapped DOX exhibited sustained drug release and greater inhibitory effect on cell viability than the free DOX drug on breast cancer cell lines.¹⁸ To further understand and develop models for optimizing this simple yet effective carrier system, we present here a systematic evaluation of the uptake and translocation properties of this nanoparticle system. Understanding the mechanisms of nanoparticle interactions with the cells of interest will result in improved

Received: August 14, 2012

Revised: October 2, 2012

Published: October 4, 2012

Scheme 1. Preparation and Structure of the Polymer Starting Material for Nanoparticle Formation

design of nanoparticles as efficient drug delivery systems and safe diagnostic imaging tools.¹⁹

In this study, Boltorn H30 hyperbranched copolymer micelles carrying PEG on the surface were hybridized with the organic dye fluorescein (fluorescein cadaverine) to form H30-(PEG_{10k})₅-FL nanoconjugates, which allow for the observation of cellular uptake by fluorescent techniques. MDA-MB468 breast cancer cells were used as a model for the study of nanoparticle uptake characteristics. The effects of time, concentration, and energy on particle uptake by MDA-MB468 cells were demonstrated, and the mechanisms of nanoparticle translocation to the cells and intracellular trafficking were also investigated. Finally, the internalization of the fluorescent nanoparticles in various types of cell cultures was studied and compared to MDA-MB468 cells.

EXPERIMENTAL SECTION

Preparation of H30-PEG_{FL} Nanoparticles. Boltorn-H30-co-(PEG_{10k})₅ copolymers were synthesized and characterized as previously described (Scheme 1).¹⁸ The Boltorn-H30-PEG10k-FL conjugates were synthesized using a two-step procedure, by first activating the hydroxyl groups of the Boltorn with succinic anhydride followed by conjugation with fluorescein cadaverine by *N*-ethyl-*N'*-dimethylaminopropylcarbodiimide/1-hydroxybenzotriazole (EDCI/HOBt) catalyzed amidation as reported by the group of Gong and co-workers.¹⁰ The resulting polymer was further purified via dialysis in a 10 kDa membrane for 4 days followed by freeze-drying. The material

was then dissolved in phosphate buffered saline solution (PBS), and the size was determined by dynamic light scattering (DLS). Average diameter: 54 ± 20 nm (DLS intensity average).

Cells and Agents. The human breast carcinoma cell lines MDA-MB468, MDA-MB23, 1 and MCF7, human kidney carcinoma cell line A498, and mouse macrophage cell line Raw 264.7 were obtained from ATCC (American Tissue Culture Collection) and maintained according to instructions. Cells were cultured in Dulbecco's Modified Eagle Medium (DMEM) supplemented with 10% fetal bovine serum, 100 units/mL penicillin, and 100 mg/mL streptomycin under 5% CO₂ at 37 °C. Cells were seeded in 12-well plates (Costa, Corning Incorporated) at the density of 2 × 10⁵ cells/well and incubated for 24 h to allow for cell attachment.

Ten kilodaltons of Dextran-rhodamine was prepared as previously described.²⁰ Cholera toxin B subunit (CTB) Alexa 647, transferrin Alexa 647, lysotracker red, and secondary antibodies were obtained from Invitrogen (Eugene, OR). Specific antibodies against early endosome marker (EEA1), and Golgi marker (TGN46), were purchased from Abcam Inc. Water, dimethyl sulfoxide (DMSO), methanol, and other HPLC-grade solvents were from Sigma-Aldrich Company, Ltd. All pharmacological inhibitors and other reagents of general laboratory grade were purchased from Sigma (St. Louis, MO) unless otherwise stated. Stock solutions were prepared and stored at -80 °C in small aliquots, as per manufacturer's recommendation.

Properties of Nanoparticle Uptake. Cells were seeded in 12-well plates at a density of 2 × 10⁵ per well and the cells were allowed to adhere for 24 h. To study the effect of incubation time, the medium was replaced with 1 mL medium containing 300 µg/mL nanoparticles (1.0 µM FL-equiv concentration), and the cells were incubated for 0,

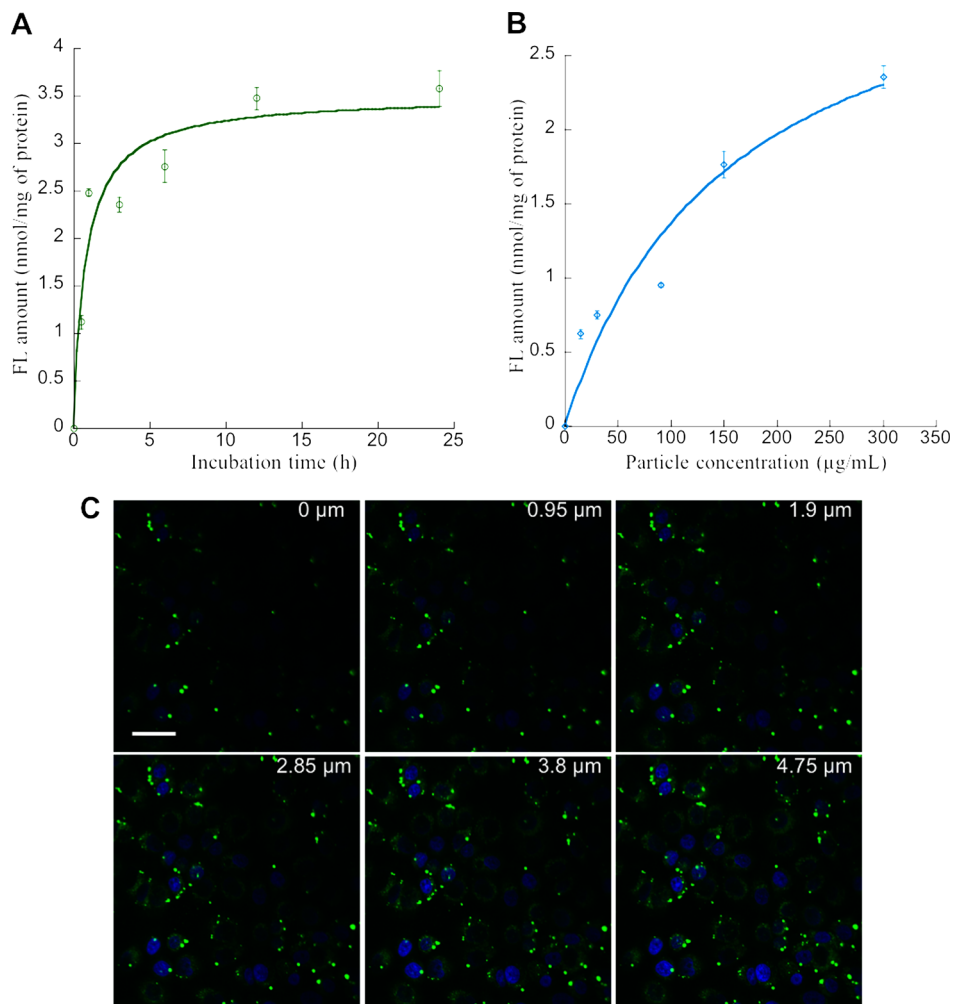


Figure 1. Uptake profiles of H30-(PEG_{10k})₅-FL nanoparticles (NP) in MDA-MB468 human breast cancer cells. (A) Time course of FL fluorescence amount (mean uptake) after incubation with 300 $\mu\text{g}/\text{mL}$ nanoparticle (with equivalent FL concentration of 1 μM) at 37 $^{\circ}\text{C}$. (B) Effects of concentration on nanoparticle uptake at 37 $^{\circ}\text{C}$ for 3 h. Points represent mean \pm SD ($n = 6$). (C) Confocal laser scanning microscopic images were taken by changing the Z-axis (0–4.75 μm) to show the location of 300 $\mu\text{g}/\text{mL}$ H30-(PEG_{10k})₅-FL in MDA-MB468 cells after 3 h incubation. Scale bar = 15 μm .

0.5, 1, 3, 6, 12, and 24 h, respectively. The half maximal uptake time was calculated by nonlinear regression analysis using KaleidaGraph v4.1 (Reading, PA). The effect of nanoparticle concentration on the cellular uptake was investigated by adding various amounts of nanoparticles (0, 15, 30, 90, 150, and 300 $\mu\text{g}/\text{mL}$) followed by a 3-h incubation, and a subsequent monitoring of the cellular uptake. The uptake results were curve-fitted to the Michaelis–Menten equation using KaleidaGrap, and the Michaelis constant (K_m) as well as the maximal uptake (V_{\max}) were determined.

After the nanoparticle treatment, the cells were washed with PBS, then with a medium at pH 4.5, and two more times with PBS. The washing protocol was performed at the end of each treatment to remove extracellular chemicals and nanoparticles that had adhered passively to the cellular plasma membrane. Next, cells were lysed in 100 μL of cell lysis buffer (Sigma) for 15 min. After centrifugation at 4 $^{\circ}\text{C}$ (16,800 g for 10 min), 10 μL of cell lysate were used to quantify protein concentration by the BCA assay. Fluorescein levels in the remaining lysate were determined using a fluorescence spectrophotometer (BioTek Synergy MX, VT) at $\lambda_{\text{Ex}} = 490 \text{ nm}$ and $\lambda_{\text{Em}} = 520 \text{ nm}$. Cellular uptake of fluorescent nanoparticles was expressed as the fluorescence intensity of nanoparticles normalized to milligram cell protein.

In the uptake experiments conducted at 4 $^{\circ}\text{C}$, the cells were washed with PBS and preincubated in serum-free RPMI 1640 medium at 4 $^{\circ}\text{C}$ for 30 min. Three hundred micrograms per milliliter of nanoparticle

solution (1.0 μM FL-equiv) was added, and the cells were incubated for 3 h either at 37 or 4 $^{\circ}\text{C}$. In all temperature- and energy-dependent uptake assays, the cell medium was serum free.

Intracellular Localization by Confocal Laser Microscopy.

MDA-MB-468 cells were seeded at semiconfluence concentrations on 12 mm coverslips in wells of a 12-well plate (BD) in a humid atmosphere supplemented with 5% CO₂ at 37 $^{\circ}\text{C}$. Cells were washed 3 times with PBS, before 1.5 mL of DMEM containing 300 $\mu\text{g}/\text{mL}$ of nanoparticles (1.0 μM FL-equiv) was added to each plate, and cells were incubated for a given period of time at 37 $^{\circ}\text{C}/5\%$ CO₂.

The cells were then washed as described above to remove the passively adhered nanoparticles, and the cells were stained with 4',6-diamidino-2-phenylindole (DAPI) by incubating the cells with the dye for 5 min, washed with PBS twice, mounted in Canadian balsam before being imaged under an Olympus FV1000 laser confocal microscope. The images were processed using FV10-ASW software.

Mechanism of Uptake and Intracellular Trafficking of Nanoparticles. To study the endocytic pathways and intracellular trafficking of the nanoparticles, MDA-MB468 cells were seeded as described above in 12-well plates. Cells were treated with 300 $\mu\text{g}/\text{mL}$ nanoparticles (1.0 μM FL-equiv) in medium and incubated for 3 h. Colocalization assays in living cells were performed in order to identify the endocytic vesicles involved in the nanoparticle internalization. Following the nanoparticle treatment, the cells were incubated with different dyes depending on the purpose of the staining: 0.1 mg/mL

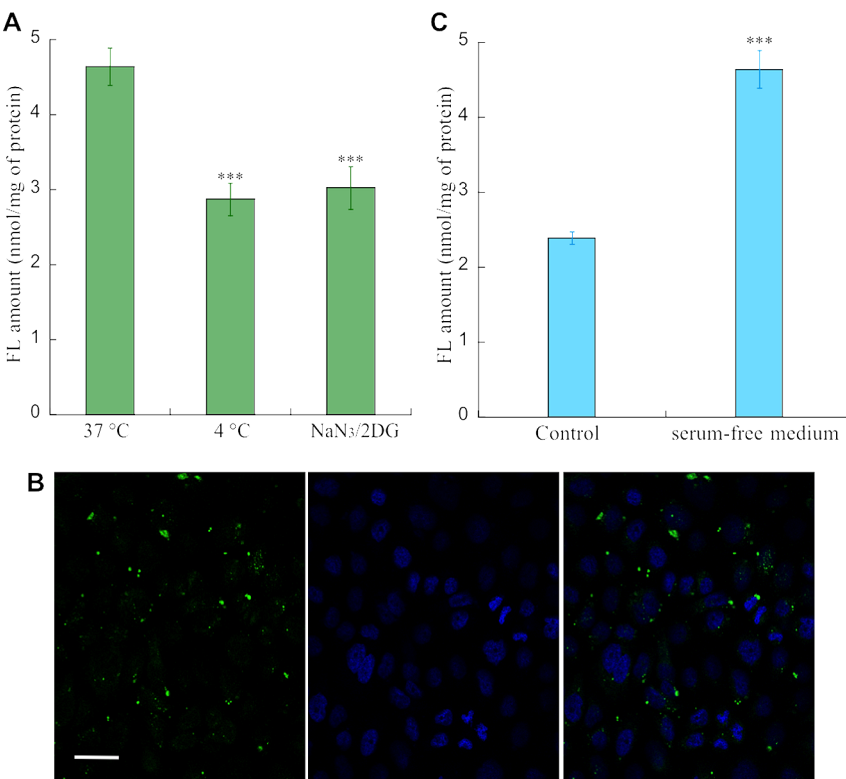


Figure 2. Role of energy and serum in endocytosis of 300 $\mu\text{g}/\text{mL}$ H30-(PEG_{10k})₅-FL (with equivalent FL concentration of 1 μM) in MDA-MB468 cells. (A) Uptake at 4 °C or in the presence of a metabolic inhibitor mixture containing 10 mM NaN₃ and 5 mM 2DG. Data represents mean \pm SD ($n = 6$). *** $p < 0.001$ when compared with 37 °C. (B) The difference in temperature dependence is confirmed via confocal microscopy. Image shows cells pretreated at 4 °C for 10 min prior to subsequent coincubation of nanoparticles (green) at 4 °C for 3 h. Nuclei are stained with DAPI (blue). Scale bar = 20 μm . (C) The effect of serum-free medium on endocytosis of particles. Data represents mean \pm SD ($n = 6$). *** $p < 0.001$ when compared with control. Data represents mean \pm SD ($n = 6$).

10 kDa dextran-rhodamine conjugate to label macropinosomes, 5 $\mu\text{g}/\text{mL}$ transferring Alexa647 conjugate to label recycling and sorting endosomes, and with 2.5 $\mu\text{g}/\text{mL}$ CTB Alexa647 conjugates to label caveolin. Cells were imaged using confocal microscopy.

Immunostaining was used to investigate nanoparticle intracellular trafficking. After 3 h of nanoparticle incubation, cells were fixed with 4% paraformaldehyde, and labeled with specific antibodies for early endosomes (EEA1) and Golgi network (TGN), respectively. Nanoparticle colocalization assay with lysotracker red was performed in order to label lysosomes. Cells were imaged using a confocal microscope.

In the endocytic inhibition assays, cells were washed with warm (37 °C) PBS, and fresh medium was added containing the endocytosis inhibitors. Next, the cells were treated with 300 $\mu\text{g}/\text{mL}$ nanoparticles either in the presence or absence of inhibitors of endocytic pathways. Various well-characterized inhibiting drugs were selected for their ability to inhibit specific steps in the endocytic pathway and were added to the cell culture media at the indicated concentrations 0.5 h prior to the addition of the H30-(PEG_{10k})₅-FL suspensions. After tests for cytotoxicity as well as efficacy, a suitable concentration for each drug was chosen. The drugs include filipin (1 $\mu\text{g}/\text{mL}$), nystatin (10 $\mu\text{g}/\text{mL}$), phenylarsine oxide (0.1 μM), chlorpromazine (1 $\mu\text{g}/\text{mL}$), amiloride-HCl (0.1 mM) and cytochalasin D (0.5 μM). The effects of lysosomotropic agents (0.1 $\mu\text{g}/\text{mL}$ baflimycin A, 1 mg/mL ammonium chloride and 1 mg/mL methylamine) on nanoparticle uptake were also studied. As confirmed by bright-field microscopy and MTT assays (results not shown), the drugs did not affect cell viability during the course of the experiment. After a 0.5-h preincubation with the drugs at 37 °C, 300 $\mu\text{g}/\text{mL}$ of the nanoparticle (1.0 μM FL-equiv) solution was added to the cells for 3 h, and then the cells were prepared for fluorescence analysis as described above.

Statistical Analysis. The uptake of nanoparticles is presented as mean values with standard deviation (SD) from three independent

experiments. Statistical analysis was performed using one-way analysis of variance (ANOVA) followed by a Tukey *posthoc* test using KaleidaGraph v4.1 (Reading, PA). In all cases, the threshold value for statistical significance was set to $p < 0.05$.

RESULTS AND DISCUSSION

We have previously reported on polyester-based nanoparticles prepared from the hyperbranched polymer Boltorn fitted with PEG chains on the surface.¹⁸ These particles were developed as a potential simpler drug delivery system for chemotherapeutics compared to monodisperse dendrimers,²¹ and their preparation is outlined in Scheme 1. In our recently published study, we found that this type of nanoparticles could be efficient carriers of the chemotherapeutic DOX, and that the delivery of DOX with these nanoparticles resulted in inducing significantly more apoptosis compared to the treatment free drug. These carriers were also found to have a positive effect on treating multi-drug-resistant breast cancer cells (results not published), suggesting that these carriers have several advantages in drug delivery applications apart from their simple preparation from commercial starting materials. In order to better understand the effects seen for these nanoparticles in cancer cells, we have herein conducted a detailed and careful investigation of the nanoparticle uptake and intracellular trafficking.

Time- and Concentration-Dependence of Nanoparticle Uptake. The uptake of nanoparticles was assessed using a breast cancer cell line (MDA-MB468) to identify the characteristics of this transport system related to intracellular drug delivery. Intracellular uptake of nanoparticles in MDA-MB468 cells was detected by fluorescence following various

incubation times. The concentration of nanoparticles ($300 \mu\text{g}/\text{mL}$) used corresponds to a polymer concentration of $5.5 \mu\text{M}$ and a conjugated fluorescein equivalent concentration $1 \mu\text{M}$, respectively, and does not significantly affect the viability of the cells at this concentration (Supporting Information). As shown in Figure 1A, cell penetration of nanoparticle occurs, and a significant internalization was detected as early as 30 min after addition of the nanoparticles at 37°C , which demonstrates that these hyperbranched polymer nanoparticles translocate rapidly into the cell, and the time for half-maximal uptake was found to be $0.8 \pm 0.2 \text{ h}$. The rapid uptake of nanoparticles during the initial accumulation can be attributed to a first-order (linear) component. Figure 1A also shows a subsequent continuous increase in uptake reaching a plateau at 10 h post-treatment.

The effects of nanoparticle concentration on nanoparticle uptake were also investigated. Various nanoparticle concentrations ranging from 0 to $300 \mu\text{g}/\text{mL}$ were applied to MDA-MB468 cells for 3 h. As shown in Figure 1B, the uptake of nanoparticles increased in a concentration-dependent manner when incubated at 37°C and followed a Michaelis–Menten model fit with a V_{\max} of $3.5 \pm 0.2 \text{ nmol FL/mg of protein}$ and a K_m of $156.3 \pm 88.3 \mu\text{g}/\text{mL}$.²² Based on the maximal uptake value (V_{\max}), MDA-MB468 cells displayed a substantial capacity for nanoparticle transport, which represented a significant fraction (18.1%) of the nanoparticle quantity applied to the cells. The Michaelis constant (K_m) shows a relatively low affinity to the cell membrane, because our K_m ($\sim 2.8 \mu\text{M}$) is in the micromolar range, whereas K_m values in the nanomolar range are considered to be of high affinity in receptor-mediated endocytosis.²³ It has been suggested that membrane affinity depends mainly on the amount of positive charge on the particle surface, and cationic particles show more affinity for negatively charged cell surface than the corresponding neutral or negative particles due to the electrostatic interactions.^{24,25} This could explain the low affinity of our nanoparticles for the cell membrane since the surface potential of the nanoparticles is negative (-21 mV). Therefore, these results indicate that active energy-dependent processes may contribute to the internalization of our nanoparticles in the breast cancer cells studied. An understanding of these profiles could lead to an improvement in the design of nanoparticles for controlled drug delivery applications.

The internalization of nanoparticles by cells was further confirmed by confocal microscopy. Figure 1C shows a sample Z-stack image of the cells treated with $300 \mu\text{g}/\text{mL}$ of nanoparticles, which confirms the particle internalization. Green fluorescence indicates that the nanoparticles were internalized and transported to the perinuclear region within 3 h, while no green fluorescence was detectable in the nucleus. Time-lapse imaging (up to 24 h) of cells treated with fluorescent nanoparticles did not reveal any further localization changes. Thus, a 3-h incubation time and a concentration of $300 \mu\text{g}/\text{mL}$ were selected as the parameters to be used in further studies.

Temperature- and Energy-Dependence of Nanoparticle Uptake. To investigate the energy dependence of cellular nanoparticle uptake, the transport of the particles was measured at either 37 or 4°C . As shown in Figure 2A, a clear reduction of the intracellular accumulation of nanoparticles was found at 4°C as compared to the experiments performed at 37°C . The cellular uptake of nanoparticles at 4°C was further examined using confocal microscopy, and Figure 2B shows a reduced intracellular fluorescence signal of the particles as

compared to the treatment at 37°C shown in Figure 1C. This effect is probably due to decreased membrane recycling at 4°C . Furthermore, a simultaneous inhibition of respiration and the glycolytic pathway by the combined exposure of the cells to nanoparticles and 10 mM sodium azide (NaN_3) as well as 5 mM 2-deoxyglucose (2DG) resulted in a significant inhibition of nanoparticle transport (Figure 2A). Reduced uptake at 4°C or in the presence of a metabolic inhibitor mixture strongly indicates that nanoparticles are internalized by an active energy-dependent process. Energy-dependent entry routes have been shown to mediate the uptake of other types of nanomaterials, such as carbon nanotubes.²⁶

Serum-Dependence of Nanoparticle Uptake. In addition, particles cultured in a serum-free medium displayed much higher levels of uptake than particles cultured in standard medium, as shown in Figure 2C. This strongly suggests that the transport of nanoparticles across the cancer cell membrane is affected by the presence of serum. It is well-known that the intracellular delivery and uptake of positively charged nanocarriers is affected by the presence of serum.²⁷ However, for the polymer in this study, with negative charge (-21 mV), the effect of serum on cell entry is also found to be significant. Unlike the positively charged nanocarriers, electrostatic interactions between negatively charged nanocarriers and the cell membrane are generally very low.^{24,25} For the nanoparticles in this study, it cannot be excluded that nanocarrier–serum protein complexes may form and interfere with the endocytic process, thus decreasing the cellular uptake of nanoparticles, as seen in Figure 2C. The average sizes of the nanoparticles were found to be 54 nm in PBS and 107 nm in medium containing 10% FBS via DLS (Supporting Information). The larger size in medium may be attributed to the protein corona on the particle surface.²⁸ Similar results have been recently shown for negatively charged gold–peptide nanoconjugate particles.²⁹

Although the presence of serum in the media modulates nanoparticle–cell interactions, it appears that these specific carriers can deliver drug cargos into the cytoplasm successfully, as published previously by our group.¹⁸ Furthermore, in vivo biodistribution experiments show that the serum half-life of DOX attached to the high molecular weight polymer is significantly increased as when compared to the free drug.⁹

Studies on the Mechanisms of Nanoparticle Uptake. In order to identify the biological compartments involved in the internalization of these polyester based nanoparticles, we performed colocalization assays with biomarkers of different endocytic vesicles. Transferrin-Alexa 647 and a caveolin (CTB-Alexa 647) were used to trace the clathrin-dependent pathway and the caveolae structure, respectively,³⁰ while dextran-rhodamine was used to label the macropinosomes.²⁴ Figure 3A shows colocalization data between the nanoparticles (green channel) and the endocytic vesicles (red channel). High colocalization (yellow vesicles) was observed with transferrin (clathrin pathway) and dextran (macropinocytosis), while no significant correlation with the CTB signal (caveolae pathway) was observed.

Nanoparticles bound specifically to macropinosomes and transferrin in cells were also confirmed by endocytic inhibition assays. Effects of pharmacological inhibitors of macropinosome-mediated endocytosis (amiloride and cytochalasin D), inhibitors of caveolae-mediated endocytosis (nystatin and filipin), or inhibitors of clathrin-mediated endocytosis (phenylarsine oxide and chlorpromazine) on the transport properties of nanoconjugates across MDA-MB-468 cell membranes were studied.

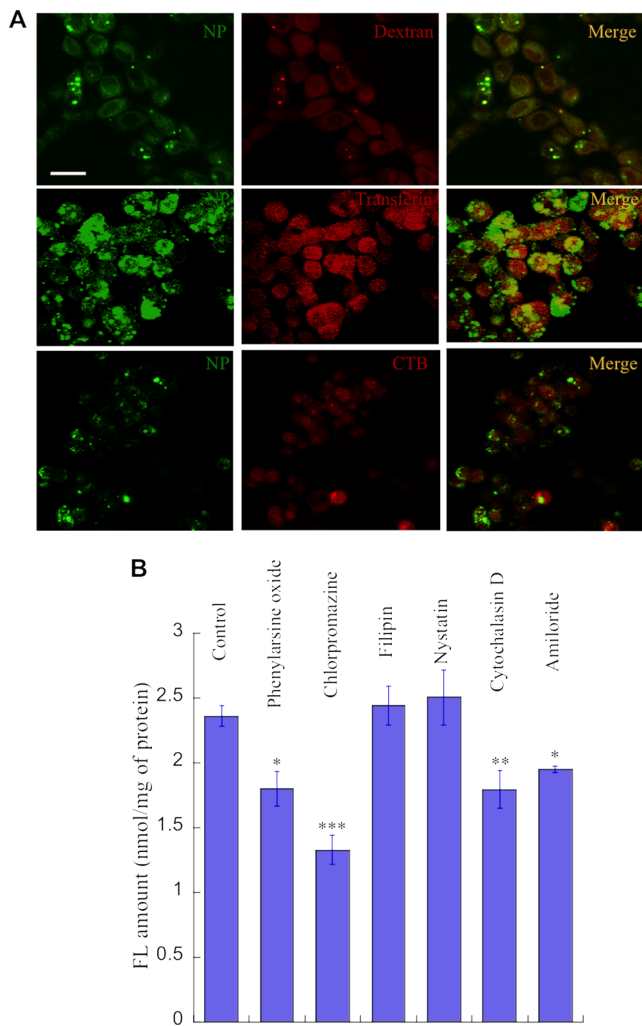


Figure 3. Role of macropinosome, clathrin-coated pits and caveolae in endocytosis of H30-(PEG_{10k})₅-FL nanoparticles in MDA-MB468 cells. (A) H30-(PEG_{10k})₅-FL nanoparticles (green) colocalization with endocytic markers (red). High colocalization (yellow vesicles) was observed with transferrin (clathrin pathway) and dextran (macropinocytosis), while no correlation with CTB signal (caveolin pathway) was observed. Scale bar = 20 μ m. (B) Effect of endocytic inhibitors on nanoparticle uptake at 37 °C for 3 h in MDA-MB468 cells. Cells were untreated (control) or pretreated with inhibitors for 30 min at 37 °C prior to addition of nanoparticles (300 μ g/mL), and the fluorescence signal was measured following incubation for 3 h at 37 °C. Data represents mean \pm SD ($n = 6$). * $p < 0.05$, ** $p < 0.01$, *** $p < 0.001$ when compared with control.

The results shown here demonstrate that there was a statistically significant decrease in both macropinocytosis and clathrin pathway-associated fluorescence in the cells as compared to cell-associated fluorescence in the absence of inhibitors (Figure 3B). Therefore, both macropinosytosis and clathrin-mediated endocytosis are likely to take place in the translocation processes of these nanoparticles across the lipid bilayer of the cell plasma membranes. This can partly be explained by nanoparticle size, which is a major parameter affecting nanoparticle endocytosis. The diameter of clathrin-coated vesicles ranges between 100 and 200 nm; caveosomes have a general diameter of approximately 60 nm, and macropinosomes are large organelles with diameters from 500 to 2000 nm.¹⁹ Since the nanoparticles in this study had a

diameter of approximately 110 nm in complex media (Table 1S), it is less likely that caveosomes could be able to transfer the nanoparticles. Therefore, clathrin-mediated endocytosis and macropinocytosis could be the primary endocytic mechanisms governed by size effects, and this claim is also supported by the experimental results showing that these two uptake mechanisms are the most significant ones in our nanoparticle uptake experiments.

Intracellular Trafficking of Nanoparticles Following Endocytosis.

Confocal imaging demonstrated that the nanoparticles are delivered to the perinuclear region as shown in Figure 1C. In order to identify the intracellular trafficking of the particles, we performed colocalization assays with EEA1, lysotracker and TGN, as known markers for early endosomes, lysosomes, and the Golgi network, respectively. As shown in Figure 4A, high colocalization of nanoparticles with lysotracker (yellow color) demonstrated that the particles are primarily transported to lysosomes following endocytosis by MDA-MB-468 cells. Conversely, a low colocalization signal is observed in EEA1 or TGN, which indicates that particles are not typically localized within early endosomes or the Golgi network.

Furthermore, the effect of lysosomotropic agents on the uptake of nanoparticles (37 °C; 3 h) was studied in order to clarify the roles of the endosomal/lysosomal compartments. Figure 4B shows that the uptake of nanoparticles by MDA-MB-468 cells was significantly inhibited by baflimycin A and ammonium chloride, although there was no statistically significant decrease in methylamine-associated fluorescence. Combined with the colocalization results, it is proposed that endosomal escape occurs in the trafficking of the nanoparticles used in this study despite the lack of any positive charges on the particles. A well-known bottleneck in drug or gene delivery into the cytosol of cells is the endosomal escape of drugs or macromolecular substances.³¹ Since our polyester-based nanoparticles do not undergo endosomal internalization, and we have previously shown an effective delivery of drugs to breast cancer cells,¹⁸ more drug-encapsulating particles are present intracellularly, and, with the exception of the fraction distributed to other subcellular compartments, more drug molecules are eventually released into the cytoplasm available to react with the target molecules.

The colocalization of nanoparticles with EEA1, lysotracker, and TGN reveals that the particles bypass early endosomes and the Golgi network, and are completely targeted to the lysosomal compartment post internalization. According to the literature, degradation of nanoparticles in lysosomes plays an important role in drug delivery in cancer cells.¹⁹ Nanoparticles are degraded into lower molecular weight fragments, and the encapsulated drug can be released through surface or bulk erosion of the degradable polymers. As shown in our previous study,¹⁸ after 24 h, the free DOX-treated cultures only had a few spots of DOX fluorescence in nuclei, while the nanoparticle-DOX-treated cultures had diffused drug fluorescence throughout the cytoplasm, which is probably caused by the unique capacity of lysosomes to facilitate sustained the drug payload release from the lysosomal compartments, which could be highly advantageous for drug delivery applications.

The exact mode of endocytosis usually determines the path of nanoparticle trafficking through various subcellular compartments.³² Similar to the case in the present study, nanoparticles internalized through clathrin-mediated endocytosis are routed to lysosomal compartments, whereas those particles internal-

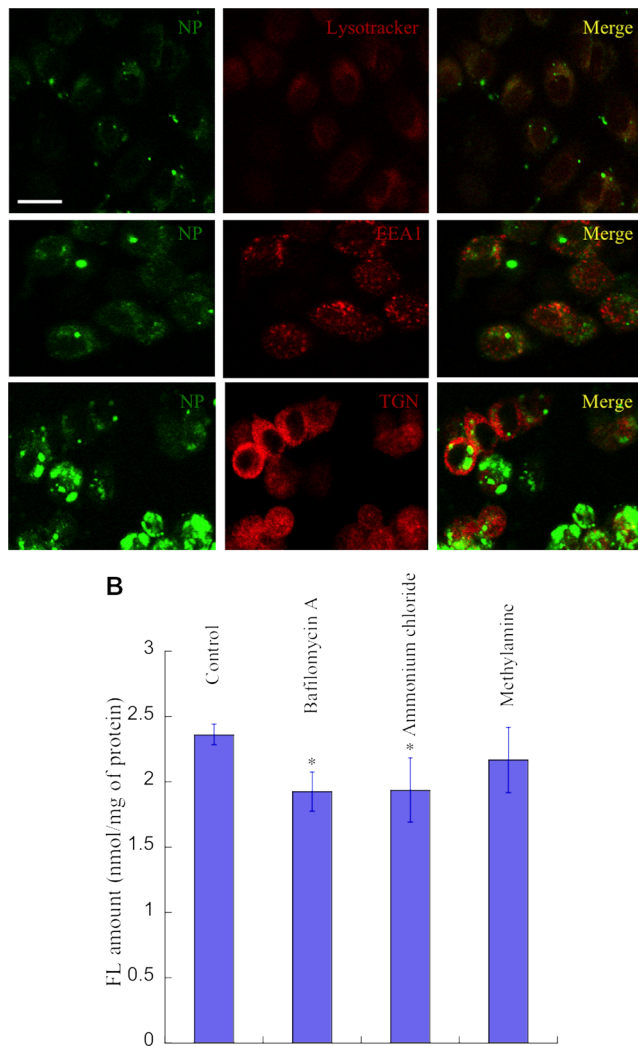


Figure 4. Intracellular trafficking of H30-(PEG_{10k})₅-FL nanoparticles after endocytosis in MDA-MB468 cells. (A) Colocalization of H30-(PEG_{10k})₅-FL nanoparticles (green) with lysotracker (lysosome marker, red), EEA1 (early endosome marker, red) and TGN46 (Golgi apparatus marker, red) after 3 h from nanoparticle treatment reveals that the particles are completely delivered to the lysosomal compartment. Scale bar = 20 μ m. (B) Effect of lysosomotropic agents (bafilomycin A, ammonium chloride and methylamine) on nanoparticle uptake at 37 °C for 3 h. Control cells were treated with 300 μ g/mL nanoparticles only. Data represents mean \pm SD ($n = 6$). * $p < 0.05$ when compared with control.

ized through the caveolae-mediated pathway have the ability to bypass lysosomes.³² Particle charge not only determines their endocytic pathways, but also influences the subsequent trafficking in cells. It was reported that anionic but not cationic nanoparticles transited through the lysosomal pathway,³³ which is consistent with our findings because of the negative surface charge of the nanoparticles. Interestingly, the endocytic properties of the cationic dendrimers resemble much that of the nanoparticles used in this study since the PAMAM dendrimers were internalized by both clathrin-dependent endocytosis and macropinocytosis but were also eventually delivered to the lysosomal compartment.²⁴ Therefore, currently unknown, complex, and dynamic mechanisms are involved in the cellular processing of nanoparticles.

Evaluation of Nanoparticle Uptake by Different Cell Lines.

In order to extend the scope of this work, we decided to

investigate the interactions of our nanoparticles with additional cell lines including mouse macrophage cells Raw 264.7, human kidney carcinoma cell line A498, and human breast cancer cell lines MDA-MB231 and MCF7. Figure 5A illustrates that these

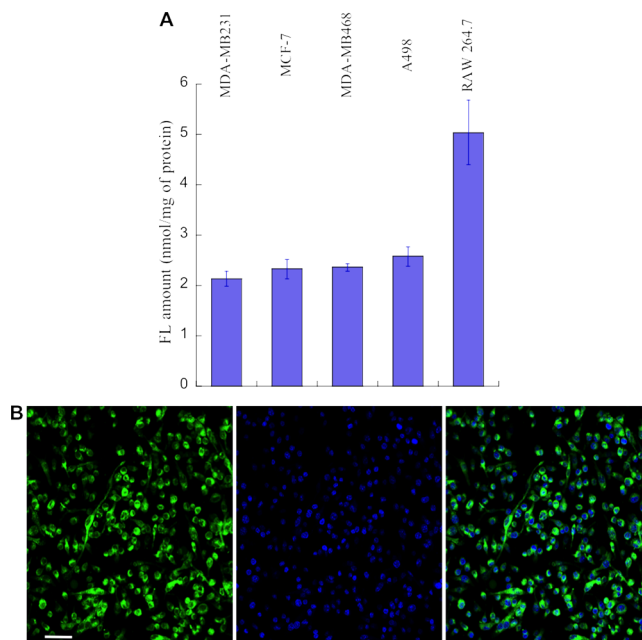


Figure 5. H30-(PEG_{10k})₅-FL endocytosis in different cell lines. (A) Different cell lines (MDA-MB231, MCF7, MDA-MB468, A498, and Raw 264.7) were treated with nanoparticles for 3 h, and uptake was measured as described in the Experimental Section. (B) Confocal imaging of RAW 264.7 cells after 3 h of treatment with nanoparticles. Strong fluorescence (green) reveals faster internalization of nanoparticles in RAW 264.7 cells. Nuclei are stained with DAPI (blue). Scale bar = 80 μ m.

different types of cell lines were all able to internalize the nanoparticles after 3 h dosing with 300 μ g/mL of nanoparticles. These measurements together with a direct comparison with MDA-MB468 cells demonstrate that the particles possess similar effects on A498 cells and other widely used breast cancer cell lines (MDA-MB231 and MCF7). However, RAW 264.7 cells showed the highest uptake of particles (double compared to the other evaluated cells) (Figure 5A). This is probably a result of the remarkable phagocytic capacity displayed by macrophages since phagosomes are rapidly recycled during the process in which cells engulf foreign particles.^{34,35}

The localization of nanoparticles in various cell lines was observed using confocal microscopy. As shown in Figure 5B, nanoparticles in RAW 264.7 cells ultimately localized in the perinuclear region, but showed strong internalization signals, which was consistent with the quantitative analysis shown in Figure 5A. MDA-MB231, MCF7, and A498 cells showed an internalization of nanoparticles in a manner analogous to what was observed in MDA-MB468 cells after 3 h. Variations in the kinetics of cellular uptake for the same type of particle in different cell lines has been reported previously.²⁴ Our data indicate that the characteristics of polyester-based nanoparticle uptake and trafficking across cell compartments are mainly dependent on the physicochemical properties of the nanoparticles since they are capable of crossing cell membranes of all tested cellular types. On the other hand, the uptake of

nanoparticles into different cell lines with different effectiveness shows that additional cellular factors may play important roles in the interaction of cells with nanomaterials.

CONCLUSIONS

Polymeric delivery systems have emerged as an important strategy to improve the efficacy and reduce the adverse effects of many drugs. In our previous study, these nanoparticles were characterized as encapsulating therapeutic agents with a potential to control the drug release and to improve the long-term retention of therapeutic drugs in breast cancer cells. In the present study, we found that the cellular uptake processes of the nanoparticles are time-, concentration-, and energy-dependent. These hyperbranched nanoparticles translocated across cell membranes via endocytosis, most likely involving clathrin- and macropinocytosis-mediated pathways. The nanoparticles did not appear to traffic to early endosomal compartments, indicating that this type of nanoparticles may offer some degree of protection to encapsulated drugs from biodegradation. Furthermore, lysosomal targeting of the nanoparticles suggests the possibility of using the lysosome as an intracellular depot in order to control drug release rates in breast cancer cells. The differences in the uptake of the particles in various cell lines shows that both intrinsic characteristics of the nanomaterials and cellular factors may influence nanoparticle–cell interaction.

In this study, we have demonstrated the uptake properties and the intracellular trafficking of a simple two-component polyester–PEG nanoparticle system. These nanocarriers may represent a valid alternative to current drug delivery systems thanks to their biocompatibility and potential for chemical modification.¹¹ We are now investigating the in vitro efficacy of these nanoparticles in drug-resistant breast cancer cells with promising initial results. Simple yet effective drug delivery systems are necessary to develop if clinical applications are to be reached in the future.

ASSOCIATED CONTENT

Supporting Information

The size, surface ζ potential, and cytotoxicity of nanoparticles. This material is available free of charge via the Internet at <http://pubs.acs.org>.

AUTHOR INFORMATION

Corresponding Author

*E-mail: andreas.nystrom@ki.se.

Notes

The authors declare the following competing financial interest(s): Andreas M. Nyström is the CEO of Polymer Factory Sweden, which commercializes bis-MPA-based dendrimers.

ACKNOWLEDGMENTS

Funding support by the Royal Swedish Academy of Sciences, the Falk Foundation, the Jeanssons Foundation, the Axel and Eva Wallströms Foundation, and the Swedish Research Council (VR), under grants 2011-3720 and 2009-3259, is gratefully acknowledged. A.M.N. is the recipient of an assistant professorship from Carl Bennet AB, the Karolinska Institutet, and Vinnova. Grants to X.Z. by the National Natural Science Foundation of China (81101688) and the Specialized Research Fund for the Doctoral Program of Higher Education

(20105301120002) are acknowledged. The authors would also thank Jakob Regberg for the preparation of the Dextrans.

REFERENCES

- Iha, R. K.; Wooley, K. L.; Nyström, A. M.; Burke, D. J.; Kade, M. J.; Hawker, C. J. *Chem. Rev.* **2009**, *109*, 5620–5686.
- Nyström, A. M.; Wooley, K. L. *Acc. Chem. Res.* **2011**, *44*, 969–978.
- Park, J. H.; Lee, S.; Kim, J. H.; Park, K.; Kim, K.; Kwon, I. C. *Prog. Polym. Sci.* **2008**, *33*, 113–137.
- Astruc, D.; Boisselier, E.; Ornelas, C. *Chem. Rev.* **2010**, *110*, 1857–1959.
- Mintzer, M. A.; Grinstaff, M. W. *Soc. Rev.* **2011**, *40*, 173–190.
- Lee, C. C.; MacKay, J. A.; Fréchet, J. M. J.; Szoka, F. C. *Nat. Biotechnol.* **2005**, *23*, 1517–1526.
- Calderon, M.; Quadir, M. A.; Sharma, S. K.; Haag, R. *Adv. Mater.* **2010**, *22*, 190–218.
- Almutairi, A.; Rossin, R.; Shokeen, M.; Hagooly, A.; Ananth, A.; Capoccia, B.; Guillaudeu, S.; Abendschein, D.; Anderson, C. J.; Welch, M. J.; Fréchet, J. M. J. *J. P. Natl. Acad. Sci. U.S.A.* **2009**, *106*, 685–690.
- De Jesus, O. L. P.; Ihre, H. R.; Gagne, L.; Fréchet, J. M.; Szoka, F. C., Jr. *Bioconjugate Chem.* **2002**, *13*, 453–461.
- Prabaharan, M.; Grailer, J. J.; Pilla, S.; Steeber, D. A.; Gong, S. Q. *Biomaterials* **2009**, *30*, 5757–5766.
- Xiao, Y. L.; Hong, H.; Javadi, A.; Engle, J. W.; Xu, W. J.; Yang, Y. A.; Zhang, Y.; Barnhart, T. E.; Cai, W. B.; Gong, S. Q. *Biomaterials* **2012**, *33*, 3071–3082.
- Prabaharan, M.; Grailer, J. J.; Pilla, S.; Steeber, D. A.; Gong, S. Q. *Biomaterials* **2009**, *30*, 3009–3019.
- Aryal, S.; Prabaharan, M.; Pilla, S.; Gong, S. Q. *Int. J. Biol. Macromol.* **2009**, *44*, 346–352.
- Pilla, S.; Kramschuster, A.; Lee, J.; Clemons, C.; Gong, S. Q.; Turng, L. S. J. *Mater. Sci.* **2010**, *45*, 2732–2746.
- Yang, X. Q.; Grailer, J. J.; Pilla, S.; Steeber, D. A.; Gong, S. Q. *Bioconjugate Chem.* **2010**, *21*, 496–504.
- Feliu, N.; Walter, M. V.; Montanez, M. I.; Kunzmann, A.; Hult, A.; Nyström, A.; Malkoch, M.; Fadeel, B. *Biomaterials* **2012**, *33*, 1970–1981.
- Malmström, E.; Johansson, M.; Hult, A. *Macromolecules* **1995**, *28*, 1698–1703.
- Zeng, X. H.; Zhang, Y. N.; Wu, Z. H.; Lundberg, P.; Malkoch, M.; Nyström, A. M. *J. Polym. Sci., Polym. Chem.* **2012**, *50*, 280–288.
- Petros, R. A.; DeSimone, J. M. *Nat. Rev. Drug Discovery* **2010**, *9*, 615–627.
- Belder, A. N. D.; Granath, K. *Carbohydr. Res.* **1973**, *30*, 375–378.
- Lee, C. C.; Gillies, E. R.; Fox, M. E.; Guillaudeu, S. J.; Fréchet, J. M. J.; Dy, E. E.; Szoka, F. C. *Proc. Natl. Acad. Sci. U.S.A.* **2006**, *103*, 16649–16654.
- Medina, S. H.; Tekumalla, V.; Cheviakov, M. V.; Shewach, D. S.; Ensminger, W. D.; El-Sayed, M. E. H. *Biomaterials* **2011**, *32*, 4118–4129.
- Schwartz, A. L.; Fridovich, S. E.; Lodish, H. F. *J. Biol. Chem.* **1982**, *257*, 4230–4237.
- Albertazzi, L.; Serresi, M.; Albanese, A.; Beltram, F. *Mol. Pharmaceutics* **2010**, *7*, 680–688.
- Perumal, O. P.; Inapagolla, R.; Kannan, S.; Kannan, R. M. *Biomaterials* **2008**, *29*, 3469–3476.
- Shi, X. H.; Von dem Bussche, A.; Hurt, R. H.; Kane, A. B.; Gao, H. J. *Nat. Nanotechnol.* **2011**, *6*, 714–719.
- Patil, S.; Sandberg, A.; Heckert, E.; Self, W.; Seal, S. *Biomaterials* **2007**, *28*, 4600–4607.
- Lundqvist, M.; Stigler, J.; Elia, G.; Lynch, I.; Cedervall, T.; Dawson, K. A. *Proc. Natl. Acad. Sci. U.S.A.* **2008**, *105*, 14265–14270.
- Wang, G. K.; Papasani, M. R.; Cheguru, P.; Hrdlicka, P. J.; Hill, R. A. *Nanomed: Nanotechnol., Biol. Med.* **2012**, *8*, 822–832.
- Sahay, G.; Kim, J. O.; Kabanov, A. V.; Bronich, T. K. *Biomaterials* **2010**, *31*, 923–933.
- De Bruin, K. G.; Fella, C.; Ogris, M.; Wagner, E.; Ruthardt, N.; Brauchle, C. J. *Controlled Release* **2008**, *130*, 175–182.

- (32) Bareford, L. A.; Swaan, P. W. *Adv. Drug Deliver. Rev.* **2007**, *59*, 748–758.
- (33) Harush-Frenkel, O.; Rozentur, E.; Benita, S.; Altschuler, Y. *Biomacromolecules* **2008**, *9*, 435–443.
- (34) Conner, S. D.; Schmid, S. L. *Nature* **2003**, *422*, 37–44.
- (35) Gagnon, E.; Duclos, S.; Rondeau, C.; Chevetaaa, E.; Cameron, P. H.; Steele-Mortimer, O.; Paiement, J.; Bergeron, J. J. M.; Desjardins, M. *Cell* **2002**, *110*, 119–131.